Circuits, Systems, and Signal Processing
https://doi.org/10.1007/s00034-023-02497-x

An Adaptive Vehicle Tracking Enhancement Algorithm Based on Fuzzy Interacting Multiple Model Robust Cubature Kalman Filtering

Guoxin Han[1,2] · Fuyun Liu[1] · Jucai Deng[3] · Weihua Bai[2] · Xiaolin Deng[4] · Keqin Li[5]

Received: 20 November 2022 / Revised: 16 August 2023 / Accepted: 18 August 2023

Abstract
Vehicle tracking is a core problem hindering multisensor fusion in intelligent driving. The interference caused by measurement outliers and motion estimation model mismatch seriously affects the estimation accuracy of target states. In view of these problems, an adaptive vehicle target tracking enhancement algorithm based on fuzzy interacting multiple model robust cubature Kalman filtering (FLIMM-IARCKF) is developed. In this algorithm, we constructed a derivative-free adaptive robust cubature Kalman filter (IARCKF) to suppress measurement outliers and errors in motion estimation modeling. Furthermore, a combined fuzzy reasoning method is developed to work with the interacting multiple model algorithm, which further enhances the target tracking performance by increasing the efficiency of model probability updating and by adaptively regulating the process noise covariance matrix. Simulated experiments verify the effectiveness of the IARCKF algorithm and reflect the advantages of the FLIMM-IARCKF algorithm in estimation accuracy, robustness, and model transformation efficiency when compared to the STCKF (Yun et al in Measurement 191:110063, 2022), Huber-CKF (Tseng et al in J Navig 70(3):527–546, 2017), MRCKF (Wu et al Acta Phys Sin 64(21):218401, 2015. https://doi.org/10.7498/aps.64.218401) and IMM-CKF (Song et al in ISA Trans 12(6):387–395, 2020) algorithms. The results show that the mean absolute percentage error (MAPE) of FLIMM-IARCKF in average position and velocity improved over the aforementioned approaches by 33.48%, and the average root-mean-square error (RMSE) improved by 32.64%. Real vehicle experiments showed that the average MAPE of FLIMM-IARCKF when used to determine position and velocity improved by 25.70%; the average RMSE improved by 28.96% when compared to the aforementioned algorithms, with an average operational time of 56.13 ms. Experimental results further revealed that FLIMM-IARCKF

✉ Guoxin Han
Hanguoxin1993vip@163.com

Published online: 02 September 2023

shows superior performance in vehicle target tracking without influencing execution efficiency.

Keywords IMM · CKF · Vehicle target · Combined fuzzy reasoning · Robust adaptive tracking

1 Introduction and Motivation

Target tracking is a core problem hindering the multisensor fusion in intelligent vehicle operations. Its difficulty lies in the optimal estimation of the target state in cases of measurement outliers and motion estimation model mismatching. To realize the state estimation of nonlinear systems, nonlinear filtering algorithms such as EKF [14], UKF [23], and CKF [5] have been proposed and widely applied. The CKF approaches the state posterior mean value and covariance of the nonlinear system through the numerical integration of the third-order spherical radial cubature criterion. The CKF exhibits higher estimation accuracy, higher computational efficiency, and better numerical stability than the EKF and UKF [15, 16]. The challenge is that CKF requires accurate posterior statistical information of known measured noise, so its estimation accuracy is seriously degraded if a measurement outlier occurs or there is significant measurement noise [19].

Given the changes in a target's motion state or the possibility of disturbances from different external environments, many measurement outliers and noise sources may be generated during target tracking. To address this problem, Huber et al. proposed a strictly derived and generalized maximum likelihood estimation method, which can weaken the weight of measurements disturbed by outliers through the Huber weight function, thus inhibiting the influence of measurement outliers on estimation accuracy [10]. Zhu et al. adaptively selected the threshold of the Huber weight function through projection statistics, aiming to further improve the robustness of Huber-UKF [31]. Chen et al. proposed a maximum experience depth function to estimate the robustness of the covariance and scatter matrix under Huber's contamination model [2]. Li et al. applied the CKF algorithm based on Huber M-estimation for motor state tracking and navigation system state estimation when significant measurement noise existed [12, 13]. Zou et al. investigated the state estimation problem for linear discrete-time systems with intermittent measurement outliers [32]. Shao et al. developed a variational Bayesian approach-based adaptive maximum correlation coefficient cubature Kalman filter, which can suppress the disturbance caused by measurement outliers to state estimation and measurement noise covariance estimation [18]. Compared to robust estimation methods such as H_∞ [3, 6], the above methods have advantages in simultaneously handling the state and measurement outliers, but they are notably disadvantaged in suppressing the errors generated by motion estimation models.

Yang et al. constructed a fading factor based on the difference between the estimated robust solutions to the measurement model and the predicted state and proposed an adaptive robust Kalman filter (ARKF) [9], which effectively inhibited the errors of the motion estimation model and has been applied to suppress the interference of measurement outliers or the robust estimation of UKF [4, 28]. Unfortunately, the traditional

fading factor needs to obtain a robust estimation solution of all the components of the state, and a substantial change in the motion state of the vehicle target can still disrupt such methods' robust estimation ability. The interacting multiple model algorithm (IMM) can realize the interaction between different motion models and solve the estimation accuracy loss triggered by the motion state change of the vehicle target during the tracking process [21, 26]. Therefore, the improved nonlinear state estimation filter was embedded into the IMM as model-conditioned filtering to further improve the estimation accuracy in some studies [8, 27]. However, the synchronous improvement and optimization of the model-conditioned filtering and the IMM algorithm have not been simultaneously considered in such studies.

To solve these problems in existing state estimation methods, an adaptive vehicle target tracking enhancement algorithm based on fuzzy interacting multiple model robust cubature Kalman filtering (FLIMM-IARCKF) is developed here. In this algorithm, a fading factor based on innovative orthogonal sequences and convex robust functions was determined to construct a derivative-free adaptive robust cubature Kalman filter, which can simultaneously suppress the influences of the errors of both measurement outliers and motion estimation models on estimation accuracy. Over this structure, a combined fuzzy reasoning method is implemented to act on the interacting multiple models algorithm, which further improves the tracking performance and estimation accuracy of the algorithm by increasing the efficiency of model probability updating and adaptively regulating the process noise covariance matrix. The resulting FLIMM-IARCKF algorithm considers multiple error factors, such as measurement outliers and motion model mismatching, as well as the corresponding improvement methods during the nonlinear tracking process of vehicle targets. It thus realizes synchronous improvements in the performance of model interaction and the accuracy of state estimation.

2 Fuzzy Interacting Multiple Model Adaptive Robust Cubature Kalman Filtering Algorithm

2.1 Improved Adaptive Robust Cubature Kalman Filtering

The CKF is a nonlinear filter that can accurately save first-order and second-order matrix information with higher estimation accuracy and numerical stability than the UKF. In the case of system state changes or measurement outliers, however, the tracking estimation performance of the CKF is substantially reduced. To improve the adaptive robust estimation performance of the nonlinear filter under system model errors, the improved fading factor and convex robust function were combined to construct a cost function of adaptive robust nonlinear filtering. Then, an improved adaptive robust cubature Kalman filtering (IARCKF) was applied.

The state equation and measurement equation for the discrete time nonlinear state space model considering additive noise are as follows:

$$x_k = f(x_{k-1}) + w_{k-1}, \quad z_k = h(x_k) + v_k \tag{1}$$

where $x_k \in R^n$ is the state of the system at time k, $y_k \in R^m$ is the measurement, and $w_{k-1} \sim N(0, Q_{k-1})$ and $v_k \sim N(R_k)$ denote the process noise and measurement noise of the dynamic system, respectively, which are mutually independent zero-mean Gaussian white noise.

2.1.1 The Cost Function of Adaptive Robust Nonlinear Filtering

To suppress the influences of measurement outliers and the errors of the motion estimation model on the estimation accuracy of the filtering algorithm, an adaptive robust cost function for nonlinear filtering is constructed by combining the fading factor using an innovative orthogonal sequence with the convex robust function.

Considered from the Bayesian maximum likelihood perspective, the state space model described in Eq. (1) can be solved by the following cost function.

$$\hat{x}_k = \arg\min(\|x_k - \hat{x}'_k\|^2_{(P'_k)^{-1}} + \|h(x_k) - z_k\|^2_{(R_k)^{-1}}) \tag{2}$$

where $\hat{x}_k$ denotes the state estimate after the measurement update, $\hat{x}'_k = \hat{x}_{k|k-1}$ denotes the state estimate before the measurement update, $P'_k = P_{k|k-1}$ is the covariance matrix of $\hat{x}'_k$, and $\|x\|^2_A = x^T Ax$.

To suppress the influence of outliers and heavier tails, the quadratic cost functions of Eq. (2) were reformulated using the fading factor δ_k and Huber convex robust function [24], and the expression of the reformulated minimization problem was obtained as follows:

$$\hat{x}_k = \arg\min\left(\left\|x_k - \hat{x}'_k\right\|^2_{(2\delta_k P'_k)^{-1}} + \sum_{j=1}^{m} \rho\left(\tau_{k,j}\right)\right) \tag{3}$$

The above minimization problem expression can be further rewritten as:

$$\hat{x}_k = \arg\min\left(\frac{1}{2\delta_k}\sum_{i=1}^{n} e^2_{k,i} + \sum_{j=1}^{m} \rho\left(\tau_{k,j}\right)\right) \tag{4}$$

where δ_k is the fading factor, $\rho(\zeta)$ denotes the convex robust function, $e_k = \left(P'_k\right)^{-\frac{1}{2}}\left(x_k - \hat{x}'_k\right)$, $\tau_k = (R_k)^{-\frac{1}{2}}(h(x_k) - z_k)$, $e_{k,i}$ denotes the i th component of e_k, and $\tau_{k,j}$ denotes the jth component of τ_k.

The derivation of the minimization problem and its implicit equations can be found in reference [1]. The solved cost function can be expressed as:

$$\hat{x}_k = \arg\min\left(\left\|x_k - \hat{x}'_k\right\|^2_{(\dot{P}'_k)^{-1}} + \|h(x_k) - z_k\|^2_{(\dot{R}_k)^{-1}}\right) \tag{5}$$

where $\|x\|^2_A = x^T Ax$; $\dot{P}'_k = \delta_k P'_k$ and $\dot{R}_k = (R_k)^{\frac{T}{2}} \Psi^{-1} (R_k)^{\frac{1}{2}}$ denote the reformulated predicted state covariance matrix and the measurement noise covariance matrix, respectively.

When $\alpha_k = 1$ and Ψ are constant, the cost function of adaptive robust nonlinear filtering is reduced to a conventional KF cost function. Therefore, the above cost function can be effectively applied to nonlinear filtering. The final cost function of the adaptive robust CKF can be expressed as:

$$\hat{x}_k = \arg\min \left(\left\| x_k - \hat{x}'_k \right\|^2_{(2\delta_k (P'_k - Q_k))^{-1}} + \sum_{j=1}^{m} \rho\left(\tau_{k,j}\right) + \left\| w_k \right\|^2_{Q_k^{-1}} \right) \tag{6}$$

2.1.2 The Improved Fading Factor

During the target tracking process, the error of the motion estimation model is the primary cause of measurement outliers. To radically reduce the measurement outliers, the fading factor δ_k was introduced through Eq. (3) to adaptively acquire an approximate time-varying gain matrix so that the residual sequence could remain orthogonal. In case of any error in the motion estimation model, $\delta_k > 1$, and P'_k gradually increased with the expansion of δ_k, thereby mitigating the influence of $\hat{x}'_k$ on $\hat{x}_k$ and improving the filtering robustness. δ_k is calculated through the following method:

$$\delta_k = \begin{cases} \delta_0, & \delta_0 > 1 \\ 1, & \delta_0 \le 1 \end{cases} \tag{7}$$

A Kalman filter combined with a traditional fading factor must yield a robust estimation solution for all the components of the state. To overcome this defect and further improve the filtering adaptivity, the fading factor δ_k was established based on the innovation sequence orthogonal principle expressed by Eq. (8) to correct the prediction error covariance in real time:

$$E\left[v_{k+j} v_k^T \right] = 0 \quad j = 1, 2, \ldots, m \tag{8}$$

where $v_k = z_k - \hat{z}_{k|k-1}$ denotes the innovation sequence at time k, and $E[\cdot]$ denotes the expected value.

The following lemma was introduced for the above system state space model and was previously presented in the literature [30]:

Lemma 1 *Let* $\gamma_k \triangleq x_k - \hat{x}_k$*; if* $O[|\gamma_k|^2] \ll O[|\gamma_k|]$*, indicating that Kalman filtering can accurately obtain the system state estimates, then* $\forall j$*:*

$$V_{j,k} = E\left[v_{k+j} v_k^T \right] = \Psi\left(k+j, \cdots, k, \hat{x}'_{k+j}, \cdots, \hat{x}'_k \right) \left(P_{x_k y_k} - K_k V_{0,k} \right) = 0 \tag{9}$$

where $P_{x_k y_k}$ denotes the cross covariance between the state and measurement vectors, K_k is the Kalman gain, and $V_{0,k} = E\left[v_k v_k^T \right]$

$$\Psi\left(k+j, \cdots, k, \hat{x}'_{k+j}, \cdots, \hat{x}'_k \right) = H_{k+j} \left[\prod_{n=k+1}^{k+j-1} \Phi_n \left(I - K_n H_n \right) \right] \Phi_k \tag{10}$$

The sufficient condition of Eq. (9) is:

$$P_{x_k y_k} - K_k V_{0,k} = 0 \tag{11}$$

The Kalman gain K_k can be denoted as $P_{x_k y_k} P_{y_k}^{-1}$, where P_{y_k} is the error covariance matrix of measurement. Thus, we obtain:

$$P_{x_k y_k} \left(I - P_{y_k}^{-1} V_{0,k} \right) = 0 \tag{12}$$

The sufficient condition of Eq. (12) is given as:

$$P_{y_k} - V_{0,k} = 0 \tag{13}$$

According to the Kalman filter principle, Eq. (13) can be derived as:

$$H_k P_k' H_k^T + R_k - V_{0,k} = 0 \tag{14}$$

If the fading factor enables Eq. (14) to be valid, v_{k+j} and v_k are approximately orthogonal. Therefore, the calculation formula for the fading factor is given as:

$$\delta_0 = \frac{\operatorname{tr}\left[V_{0,k} - R_k \right]}{\operatorname{tr}\left[H_k P_k' H_k^T \right]} \tag{15}$$

Equation (15) holds for linearized systems. Nevertheless, the linearization term $H_k P_k' H_k^T$ can be approximately expressed using nonlinear methods such as CKF. Thus, δ_0 can be formulated as:

$$\delta_0 = \frac{\operatorname{tr}\left[V_{0,k} - \lambda R_k \right]}{\operatorname{tr}\left[P_{y_k} - \lambda R_k \right]} \tag{16}$$

To improve the smoothing effect of state estimation, the softening factor [30] λ is introduced into Eq. (16), $\lambda \geq 1$.

The iterative calculation of the residual covariance matrix $V_{0,k}$ in Eq. (16) can be expressed as follows:

$$V_{0,k} = E\left[v_k v_k^T \right] = \begin{cases} v_k v_k^T & k = 1 \\ \frac{\mu V_{0,k-1} + v_k v_k^T}{1+\rho} & k > 1 \end{cases} \tag{17}$$

where μ is a forgetting factor usually taken as 0.95.

The adaptive robust nonlinear cost function introduced with the improved fading factor is suitable for nonlinear Gaussian filtering, such as UKF and CKF, which enhances the adaptivity and robustness of filtering while reducing the number of filtering iterations. Furthermore, this cost function can effectively suppress the influences of the measurement outlier and motion estimation model errors on the estimation accuracy, even if the robust estimation solution of all the components of the state cannot be acquired.

2.1.3 Derivation of the IARCKF Algorithm

Assuming that the optimal estimation $\hat{x}_{k-1}$ and state covariance matrix P_{k-1} of time $k-1$ are already obtained at time k, then the state estimation process of the IARCKF within one cycle is as follows:

Step 1: Time update

Calculation of cubature points:

$$X_{i,k-1|k-1} = \sqrt{P_{k-1|k-1}}\xi_i + \hat{x}_{k-1|k-1} \quad i = 1, 2, \ldots, 2n \tag{18}$$

where

$$\xi_i = \sqrt{n}\left\{\begin{bmatrix}1\\0\\\vdots\\0\end{bmatrix}, \begin{bmatrix}0\\1\\\vdots\\0\end{bmatrix}, \cdots, \begin{bmatrix}0\\0\\\vdots\\1\end{bmatrix}\begin{bmatrix}-1\\0\\\vdots\\0\end{bmatrix}\begin{bmatrix}0\\-1\\\vdots\\0\end{bmatrix}, \cdots, \begin{bmatrix}0\\0\\\vdots\\-1\end{bmatrix}\right\}_i \tag{19}$$

According to the nonlinear system model, the nonlinear propagation of cubature points can be determined as follows:

$$X^*_{i,k|k-1} = \Phi_k f\left(X_{i,k-1|k-1}\right) \quad i = 1, 2, \cdots, 2n \tag{20}$$

Prediction of the state

$$\hat{x}_{k|k-1} = \frac{1}{2n}\sum_{i=1}^{2n} X^*_{i,k|k-1} \tag{21}$$

Step 2: Robust correction

Calculate the state cubature points following the time update:

$$X_{i,k|k-1} = \sqrt{P_{k|k-1}}\xi_i + \hat{x}_{k|k-1} \quad i = 1, 2, \cdots, 2n \tag{22}$$

Evaluate the propagated cubature points:

$$Z_{i,k|k-1} = h\left(X_{i,k|k-1}\right) \quad i = 1, 2, \cdots, 2n \tag{23}$$

Calculation of predicted measurement:

$$\hat{z}_{k|k-1} = \frac{1}{2n}\sum_{i=1}^{2n} Z_{i,k|k-1} \tag{24}$$

Modified measurement covariance update:

$$\tau_k = (R_k)^{-\frac{1}{2}}\left(\hat{z}_{k|k-1} - z_k\right) \tag{25}$$

$$\Psi = \operatorname{diag}\left[\Psi_{k,j}\left(\varepsilon_{k,j}\right)\right] \quad j = 1, 2, \ldots, m \tag{26}$$

$$\hat{R}_k = (R_k)^{\frac{T}{2}} \Psi^{-1} (R_k)^{\frac{1}{2}} \tag{27}$$

Step 3: Fading factor update

The minimum variance estimate for the residuals of the state estimate is expressed as:

$$\mathrm{MMSE}[x_k] = \mathrm{tr}\left(E\left[\left(x_k - \hat{x}_k\right)\left(x_k - \hat{x}_k\right)^T\right]\right)_{\min} \tag{28}$$

To adaptively acquire an appropriate time-varying gain matrix K_k, it is required that the residual sequence ε output at different moments always remains orthogonal. The principle of an innovative orthogonal sequence constructed based on Eq. (8) is expressed as follows:

$$E\left[\varepsilon_{k+j}, \varepsilon_k^T\right] = 0 \quad j = 1, 2, \ldots, m \tag{29}$$

In view of the state space model described by Eq. (1), let $\gamma_k \triangleq x_k - \hat{x}_k$; if $O[|\gamma_k|^2] \ll O[|\gamma_k|]$, then:

$$\begin{aligned} V_{j,k} &= E\left[\varepsilon_{k+j}, \varepsilon_k^T\right] \\ &= H\left(\hat{x}_{k+j}^-\right) \cdot F\left(\hat{x}_{k+j-1}\right) \cdot \left[I - K_{k+j} H\left(\hat{x}_{k+j-1}^-\right)\right] \cdot F\left(\hat{x}_{k+j-2}\right) \\ &\quad \cdot \left[I - K_{k+j} H\left(\hat{x}_k^-\right)\right] \cdot F\left(\hat{x}_k\right) \cdot \left(P_{zz,k} - K_k V_{0,k}\right) = 0 \end{aligned} \tag{30}$$

where $H(\cdot)$ and $F(\cdot)$ denote the Jacobian matrices of $h(x_k)$ and $f(x_k)$ with respect to x_k, respectively.

The sufficiency condition of Eq. (30) is:

$$P_{zz,k} - K_k V_{0,k} = 0 \tag{31}$$

According to the derivation of Eqs. (11)–(15), the fading factor δ_k is updated:

$$\delta_k = \begin{cases} \delta_0, & \delta_0 > 1 \\ 1, & \delta_0 \le 1 \end{cases} \tag{32}$$

$$\delta_0 = \frac{\mathrm{tr}\left[V_{0,k} - R_k\right]}{\mathrm{tr}\left[\frac{1}{2n}\sum_{i=1}^{2n}\left(Z_{i,k} - \hat{z}_k\right)\left(Z_{i,k} - \hat{z}_k\right)^T\right]} \tag{33}$$

$$V_{0,k} = E\left[\varepsilon_k \varepsilon_k^T\right] = \begin{cases} \varepsilon_k \varepsilon_k^T & k = 1 \\ \frac{\mu V_{0,k-1} + \varepsilon_k \varepsilon_k^T}{1+\rho} & k > 1 \end{cases} \tag{34}$$

where $\varepsilon_k = z_k - \hat{z}_{k|k-1}$, and μ is the forgetting factor.

Step 4: Measurement update

We estimate the predicted error covariance matrix, the innovation covariance matrix and the cross covariance matrix based on the modified measurement covariance matrix

and the fading factor at time k.

$$P_{k|k-1} = \delta_k \left[\frac{1}{2n} \sum_{i=1}^{2n} \left(X^*_{i,k|k-1} - \hat{x}_{k|k-1} \right) \left(X^*_{i,k|k-1} - \hat{x}_{k|k-1} \right)^T + Q_{k-1} \right] \tag{35}$$

$$P_{zz,k|k-1} = \delta_k \left[\frac{1}{2n} \sum_{i=1}^{2n} \left(Z_{i,k|k-1} - \hat{z}_{k|k-1} \right) \left(Z_{i,k|k-1} - \hat{z}_{k|k-1} \right)^T \right] + \hat{R}_k \tag{36}$$

$$P_{xz,k|k-1} = \delta_k \left[\frac{1}{2n} \sum_{i=1}^{2n} \left(X_{i,k|k-1} - \hat{x}_{k|k-1} \right) \left(Z_{i,k|k-1} - \hat{z}_{k|k-1} \right)^T \right] \tag{37}$$

Finally, we calculate the measurement update:

$$K_k = P_{xz,k|k-1} P^{-1}_{zz,k|k-1} \tag{38}$$

$$\hat{x}_{k|k} = \hat{x}_{k|k-1} + K_k (z_k - \hat{z}_{k|k-1}) \tag{39}$$

$$P_{k|k} = P_{k|k-1} - K_k P_{zz,k|k-1} K_k^T \tag{40}$$

2.2 Interacting Multiple Model Adaptive Robust Cubature Kalman Filtering

During the vehicle tracking process, the motion state of the target vehicle is changed according to its maneuvering needs. The filtering algorithm based on a single-motion estimation model remains limited in terms of adaptivity and estimation accuracy under the maneuvering state of the vehicle target. Substantial changes in the vehicle target's motion state can still disrupt the IARCKF algorithm's robust estimation ability. According to different motion states, vehicle motion estimation models mainly include constant velocity (CV), constant acceleration (CA), and constant turn rate (CT) models [17]. The IMM algorithm can parallelly fuse multiple possible motion state models of the vehicle target and realize the interaction between motion models via the Markov chain. To improve the adaptivity and estimation accuracy of the IARCKF algorithm in the event of a vehicle target's wide-range maneuvering, an adaptive robust cubature Kalman filtering algorithm based on interacting multiple models (IMM-IARCKF) was implemented. The recursive process of the IMM-IARCKF algorithm from time $k-1$ to time k is as follows:

(1) Interactive computing input
The model conditions were initialized as follows. The matching probability of model i at time $k-1$ is known to be μ^i_{k-1}, and the target state estimation and error covariance matrix are $\hat{x}^i_{k-1|k-1}$ and $P^i_{k-1|k-1}$, respectively. The transition probability of model i to model j is $\pi_{ij}(i, j = 1, 2, 3, \cdots, n) \in (0, 1)$, and $\sum_{i=1}^{n} \pi_{ij} = 1$. The target state estimation results at time $k-1$ were weighted and mixed to acquire the input quantities $\bar{x}^j_{k-1|k-1}$ and $\bar{P}^j_{k-1|k-1}$ of IARCKF filtering

under different model matches.

$$\mu_{k-1}^{i|j} = \frac{\pi_{ij}\mu_{k-1}^{i}}{\mu_{k|k-1}^{j}} \tag{41}$$

$$\mu_{k|k-1}^{j} = \sum_{i=1}^{n} \pi_{ij}\mu_{k-1}^{i} \tag{42}$$

$$\bar{x}_{k-1|k-1}^{j} = \sum_{i=1}^{n} \hat{x}_{k-1|k-1}^{i}\mu_{k-1}^{i|j} \tag{43}$$

$$\begin{aligned}\bar{P}_{k-1|k-1}^{j} = \sum_{i=1}^{n} \Bigg[& P_{k-1|k-1}^{i} + \left(\bar{x}_{k-1|k-1}^{j} - \hat{x}_{k-1|k-1}^{i}\right) \\ & \cdot \left(\bar{x}_{k-1|k-1}^{j} - \hat{x}_{k-1|k-1}^{i}\right)^{T} \Bigg] \mu_{k-1}^{i|j}\end{aligned} \tag{44}$$

(2) Model condition filtering
The mixed estimation $\bar{x}_{k-1|k-1}^{j}$ and covariance $\bar{P}_{k-1|k-1}^{j}$ obtained through interactive computing were input into model-conditioned filtering of different model matches. The state estimation $\hat{x}_{k|k}^{j}$ and error covariance estimation $P_{k|k}^{j}$ of the target at time k were updated, and the updating results were input into the estimation fusion module.

(3) Model probability updating
Each model probability was updated to calculate the likelihood function L_k^j and realize a probability update μ_k^j of the model j as:

$$L_k^j = \frac{\exp\left[-\frac{1}{2}(\tilde{z}_k^j)^T (P_k^j)^{-1} \tilde{z}_k^j\right]}{\left|2\pi S_k^j\right|^{\frac{1}{2}}} \tag{45}$$

$$\mu_k^j = \frac{L_k^j \mu_{k|k-1}^j}{\sum_{j=1}^{n} L_k^j \mu_{k|k-1}^j} \tag{46}$$

The measurement residuals $\tilde{z}_k^j$ and residual covariance matrix S_k^j are calculated as follows:

$$\tilde{z}_k^j = z_k - \hat{z}_{k|k-1}^j \tag{47}$$

$$S_k^j = P_{zz,k|k-1}^j \left(P_{zz,k|k-1}^j\right)^T \tag{48}$$

(4) Estimation fusion
Combining the filtering updating results of each model condition, the total state

estimation $\hat{x}_{k|k}$ and error covariance matrix $P_{k|k}$ at time k were updated.

$$\hat{x}_{k|k} = \sum_{j=1}^{n} \hat{x}_{k|k}^{j} \mu_k^j \tag{49}$$

$$P_{k|k} = \sum_{j=1}^{n} \left[P_{k|k}^{j} + \left(\hat{x}_{k|k} - \hat{x}_{k|k}^{j} \right) \left(\hat{x}_{k|k} - \hat{x}_{k|k}^{j} \right)^T \mu_k^j \right] \tag{50}$$

2.3 Derivation of the FLIMM-IARCKF Algorithm

Considering the high frequency of sudden changes in the vehicle target's motion state under complex road conditions, the frequency of model probability transitions of the IMM-IARCKF algorithm should be greatly increased under such conditions. To further enhance the tracking performance of the IMM-IARCKF in the case of sudden changes in the target motion state, a combined fuzzy reasoning method is designed to act on the IMM in this section, thus further realizing the adaptive robust cubature Kalman filtering algorithm based on the fuzzy interacting multiple model (FLIMM-IARCKF). The FLIMM-IARCKF algorithm can adaptively calculate the reasonable adjustment coefficient of the process noise covariance matrix while improving the response efficiency and convergence rate of model probability updating. The structural diagram of the FLIMM-IARCKF algorithm is exhibited in Fig. 1.

The FLIMM-IARCKF algorithm constitutes a combined fuzzy reasoning system (S_1, S_2) that acts on the IMM. S_1 introduced the model probability update module to optimize the response to probability updating, and S_2 acted upon model conditioned filtering, which calculates the process noise covariance adjustment coefficient in real time and realizes the adaptive adjustment of the process noise covariance matrix.

Assuming that the motion target was converted between CV and CT models, the corresponding variables input into the model probability update module were L_k^1 and L_k^2. The model probabilities were calculated using the conventional IMM algorithm as μ_k^1 and μ_k^2, respectively. The following expressions are obtained according to Eq. (46):

$$\begin{cases} \mu_k^1 = \dfrac{L_k^1 \mu_{k|k-1}^1}{L_k^1 \mu_{k|k-1}^1 + L_k^2 \mu_{k|k-1}^2 + L_k^3 \mu_{k|k-1}^3} \\ \mu_k^2 = \dfrac{L_k^2 \mu_{k|k-1}^2}{L_k^1 \mu_{k|k-1}^1 + L_k^2 \mu_{k|k-1}^2 + L_k^3 \mu_{k|k-1}^3} \end{cases} \tag{51}$$

where $\mu_{k|k-1}^1 = \pi_{11}\mu_{k-1}^1 + \pi_{21}\mu_{k-1}^2 + \pi_{31}\mu_{k-1}^3$ and $\mu_{k|k-1}^2 = \pi_{12}\mu_{k-1}^1 + \pi_{22}\mu_{k-1}^2 + \pi_{32}\mu_{k-1}^3$.

2.3.1 The Solving Method of Model Probability Update

The fuzzy reasoning system S_1 optimized μ_k^1 and μ_k^2 to improve the response efficiency of model probability updating and the filtering convergence speed. With the optimization of μ_k^1 as an example, the input variables in system S_1 were set as S_1 and

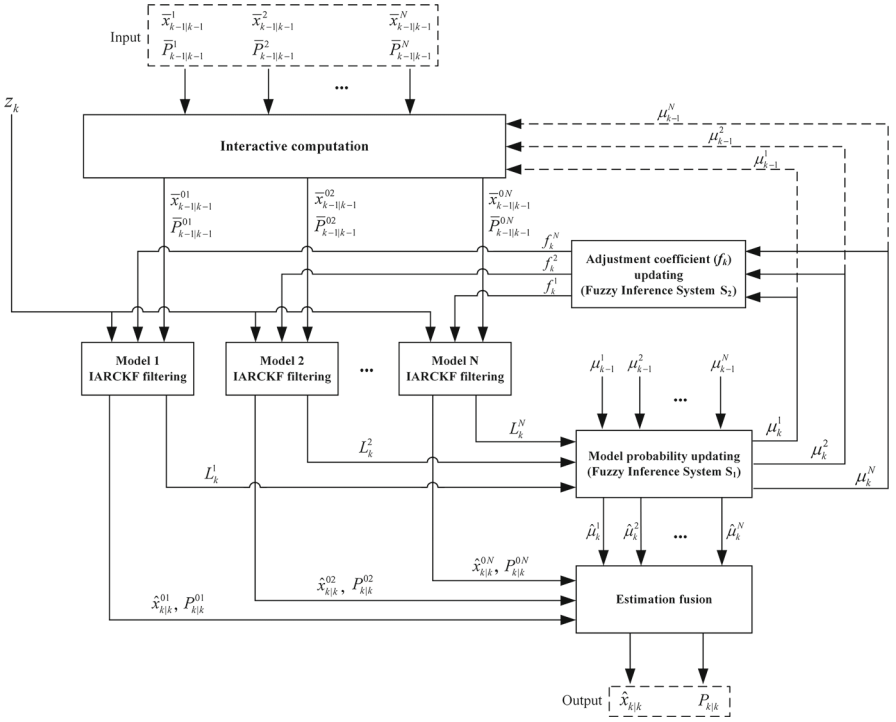

Fig. 1 The structural diagram of the FLIMM-IARCKF algorithm

F_2, and the optimized model probability $\hat{\mu}_k^j$ served as the output variable E, set:

$$\begin{cases} F_1 = \mu_{k-1}^1 \\ F_2 = \mu_k^1 - \mu_{k-1}^1 \\ E = \hat{\mu}_k^1 \end{cases} \tag{52}$$

The fuzzy domain of input variable F_1 is [0, 1], and the fuzzy subset is $\{FL$ (small), FM (medium), and FH (large)$\}$. The fuzzy domain of F_2 is $[-1, 1]$, and its fuzzy subset is $\{FN$ (negative), FZ (zero), FP (positive)$\}$. The fuzzy domain of output variable E is [0, 1], and its fuzzy subset is $\{EL$ (small), EM (medium), and EH (large)$\}$. The membership function of each variable in the fuzzy domain is displayed in Fig. 2.

Fuzzy logic rules were established according to the operation relations between input and output variables. When the variable value F_2 of the model probability was negative, the current model probability E was smaller than the model probability F_1 at the previous moment; when $F_2 = 0$, the current model probability E was equal to the model probability F_1 at the previous moment; and when $F_2 > 0$, the current model probability E was greater than the model probability F_1 at the previous moment. The fuzzy logic rules of system S_1 are listed in Table 1.

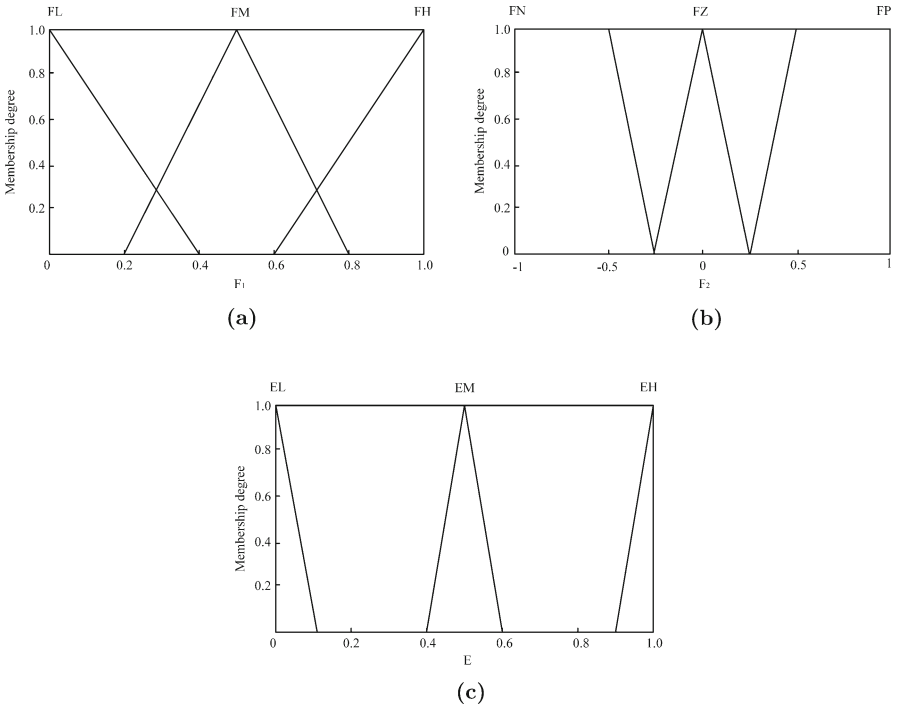

Fig. 2 The membership function of each variable in S_1

Table 1 The fuzzy logic rules of S_1

Rule numbers	F_1	F_2	E
1	FN	FL	EL
2	FN	FM	EL
3	FN	FH	EM
4	FZ	FL	EL
5	FZ	FM	EM
6	FZ	FH	EH
7	FP	FL	EM
8	FP	FM	EH
9	FP	FH	EH

Finally, the fuzzy reasoning system S_1 was processed using defuzzification by the centroid method, and the fuzzy logic reasoning result was converted into a clear value to update the model probabilities $\hat{\mu}_k^j$ in real time.

Based on this optimization of model probability updating in system S_1, the estimated fusion calculation of the IMM algorithm in Eqs. (49)–(50) was also optimized and

updated.

$$\hat{x}_{k|k} = \sum_{j=1}^{n} \hat{x}_{k|k}^{j} \hat{\mu}_{k}^{j} \tag{53}$$

$$P_{k|k} = \sum_{j=1}^{n} \left[P_{k|k}^{j} + \left(\hat{x}_{k|k} - \hat{x}_{k|k}^{j} \right) \left(\hat{x}_{k|k} - \hat{x}_{k|k}^{j} \right)^{T} \hat{\mu}_{k}^{j} \right] \tag{54}$$

2.3.2 The Adaptive Regulation Method of the Process Noise Covariance Matrix

The fuzzy reasoning system S_2 aimed to acquire the adjustment coefficient f_k of the process noise covariance matrix and acted on model conditioned filtering IARCKF. In S_2, the input variables were set as T_1 and T_2, and the output variable was set as M:

$$\begin{cases} T_1 = \mu_k^1 \\ T_2 = \mu_k^2 \\ M = f_k \end{cases} \tag{55}$$

where the fuzzy domain of input variables T_1 and T_2 is [0, 1], the fuzzy subset of T_1 is $\{TO_1$ (less), TL_h1 (little), TM_1 (medium), TH_1 (large), TE_1 (larger)$\}$ and that of T_2 is $\{TO_2$ (less), TL_2 (little), TM_2 (medium), TH_2 (large), TE_2 (larger)$\}$. The output variable M indicates the adjustment coefficient for the process noise covariance matrix of two model-conditioned filters, with a fuzzy domain of [0, 5] and a fuzzy subset of $\{MO$ (less), ML (little), MH (large), ME (larger)$\}$. The membership function of each variable in the domain is displayed in Fig. 3.

Fuzzy logic rules were established according to the influence of the process noise covariance Q on filtering estimation accuracy. When the probability result of one model is large and the probability result of the other model is small, the motion estimation model selected by the current model condition filter conforms to the actual motion state of the target. In this case, the smaller the process noise covariance is, the higher the tracking accuracy. Thus, the coefficient f_k should be appropriately reduced. Conversely, when the probabilities of each model are similar, all motion estimation models are inconsistent with the actual motion state of the tracking target. In this case, the higher the process noise covariance is, the higher the tracking accuracy, so the coefficient f_k should be appropriately increased. Finally, to prevent the model probability updating from being influenced by errors in the case of motion state changes of the vehicle target, the consistency of the process noise covariance coefficient f_k of different models should be maintained. These fuzzy logic rules of system S_2 are presented in Table 2.

The fuzzy reasoning system S_2 was processed using defuzzification by the centroid method, thus obtaining the adjustment coefficient f_k for the process noise covariance matrix in real time. Based on the fuzzy reasoning system S_2, Eq. (35) is further

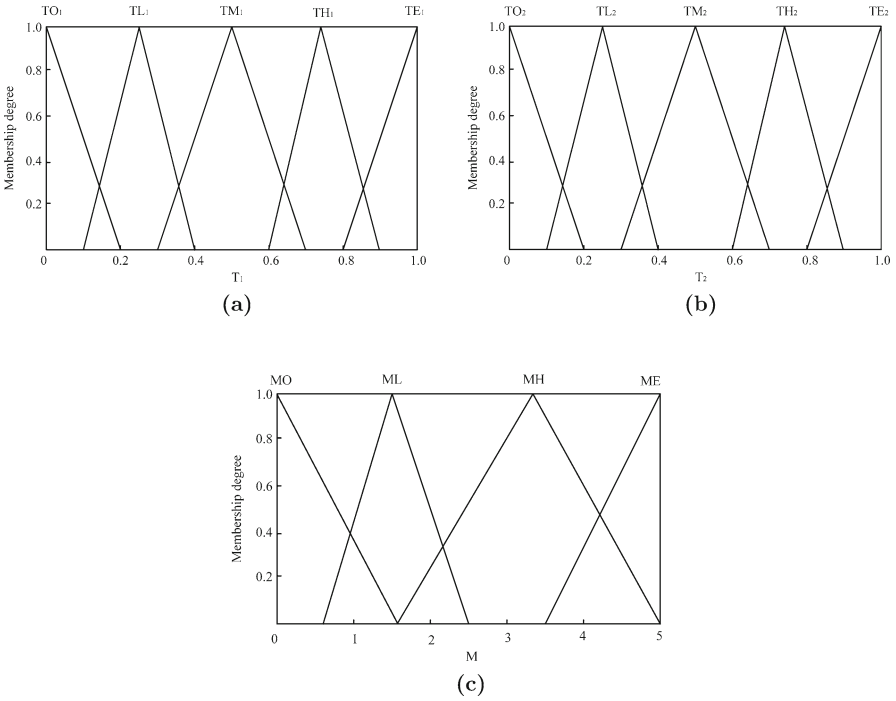

Fig. 3 The membership function of each variable in S_2

Table 2 The fuzzy logic rules of S_2

Rule numbers	T_1	T_2	M
1	TO_1	TH_2	ML
2	TO_1	TE_2	MO
3	TL_1	TH_2	MH
4	TL_1	TE_2	ML
5	TM_1	TL_2	ME
6	TM_1	TM_2	ME
7	TM_1	TH_2	MH
8	TH_1	TO_2	ML
9	TH_1	TL_2	MH
10	TH_1	TM_2	ME
11	TE_1	TO_2	MO
12	TE_1	TL_2	ML

improved into the following form:

$$P_{k|k-1} = \delta_k \left[\frac{1}{2n} \sum_{i=1}^{2n} \left(X^*_{i,k|k-1} - \hat{x}_{k|k-1} \right) \left(X^*_{i,k|k-1} - \hat{x}_{k|k-1} \right)^T + f_{k-1} Q_{k-1} \right] \tag{56}$$

3 Simulation Experiment and Results Analysis

3.1 Tracking Scenario and Parameter Setting

To verify the advantages of the algorithm designed in this study compared to competing approaches for target tracking performance, the tracking problem of a maneuvering target in the 2D rectangular plane coordinate system with a radar as the origin was considered in a simulation experiment. In this simulation, MATLAB 2020a and a laptop with an Intel i7 − 11800H processor are used as the hardware and software platforms. Meanwhile, the motion estimation models of CV (constant velocity), CTL (constant left turn rate), and CTR (constant right turn rate) were used for the interaction calculation. The system state vectors can be expressed as $x_k = [x_k, \dot{x}_k, y_k, \dot{y}_k]^T$. The system state equations under the CV and CT models are defined as follows:

$$x_k = F_{CV} \cdot x_{k-1} + \omega_{CV} \tag{57}$$

$$x_k = F_{CT} \cdot x_{k-1} + \omega_{CT} \tag{58}$$

where F_{CV} denotes the state transition matrix of the CV model, F_{CT} denotes the state transition matrix of the CTL and CTR models, and ω_{CV} and ω_{CT} are the process noise. The parameter expressions of F_{CV}, F_{CT}, ω_{CV}, and ω_{CT} can be found in reference [11].

To measure the distance and angular velocity of the target, the measurement equation of the system can be defined as:

$$z_k = \begin{bmatrix} r_k \\ \varphi_k \end{bmatrix} + v_k = \begin{bmatrix} \sqrt{(x_k - x_o)^2 + (y_k - y_o)^2} \\ \arctan\left(\frac{y_k - y_o}{x_k - x_o}\right) \end{bmatrix} + v_k \tag{59}$$

where (x_k, y_k) is the current position of the target. (x_o, y_o) is the position of the radar, which is defined as the origin of the coordinate system, and v_k is the measurement noise.

The measurement noise covariance matrix of the system is $R_k = \text{diag}\left[\left(50^2, 0.1^2\right)\right]$, where the error standard deviations of the measurement distance and angle of the observation radar are 50 m and 0.1°, respectively. The initial probability of each model is $\mu_0 = \left(1/3\ 1/3\ 1/3\right)^T$, and the Markov probability transfer matrix is P.

$$P = \begin{bmatrix} 0.8 & 0.1 & 0.1 \\ 0.1 & 0.8 & 0.1 \\ 0.1 & 0.1 & 0.8 \end{bmatrix} \tag{60}$$

To fully verify the advantages and characteristics of our algorithm in terms of estimation accuracy and robustness, the moving target in a high-speed wide-range maneuvering state was tracked in the simulation, where the radar is in a fixed position to track the target. The initial state of the target is $x_0 = \left[300\text{ m }70\text{ m/s }200\text{ m }0\text{ m/s}\right]^T$. The sampling interval of the radar is $T = 1$ s, and the total observation time is 170 s.

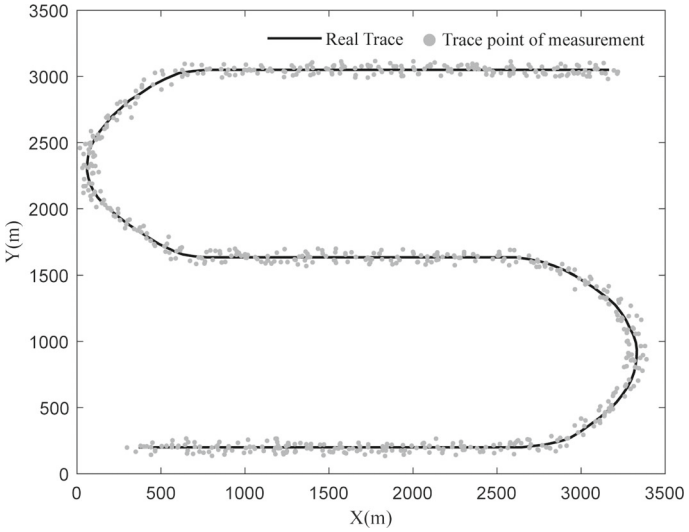

Fig. 4 The true trajectory of the vehicle target and the point tracks of radar measurement

The motion process of the target is as follows: at 1 s–40 s, 76 s–100 s, and 136 s–175 s, the target moves with uniform linear motion: at 41 s–75 s, the target makes a uniform left turn motion with an angular velocity of $\pi/30$ rad/s; and at 101 s–135 s, the target makes a uniform right turn motion with an angular velocity of $-\pi/30$ rad/s. The trajectory of the vehicle target and the point tracks of the radar measurement are shown in Fig. 4.

3.2 Experimental Results and Analysis

The simulation experiment was performed through the Monte Carlo method. The target tracking performance of the proposed method was verified by comparing it with the existing improved cubature Kalman filtering algorithms. The mean absolute percentage error (MAPE) and root-mean-square error (RMSE) were taken as the indices to measure the estimation accuracy of the filtering algorithm.

$$\mathrm{MAPE} = \frac{1}{N}\sum_{k=1}^{N}\left(\left|\frac{\hat{x}_k - x_k}{x_k}\right| + \left|\frac{\hat{y}_k - y_k}{y_k}\right|\right) \times 100\% \tag{61}$$

$$\mathrm{RMSE} = \sqrt{\frac{1}{N}\sum_{k=1}^{N}\left(\left(\hat{x}_k - x_k\right)^2 + \left(\hat{y}_k - y_k\right)^2\right)} \tag{62}$$

where $\left(\hat{x}_k, \hat{y}_k\right)$ and (x_k, y_k) denote the optimal estimation value and true value of the target position or velocity, respectively, and $N = 100$ represents the number of Monte Carlo simulations.

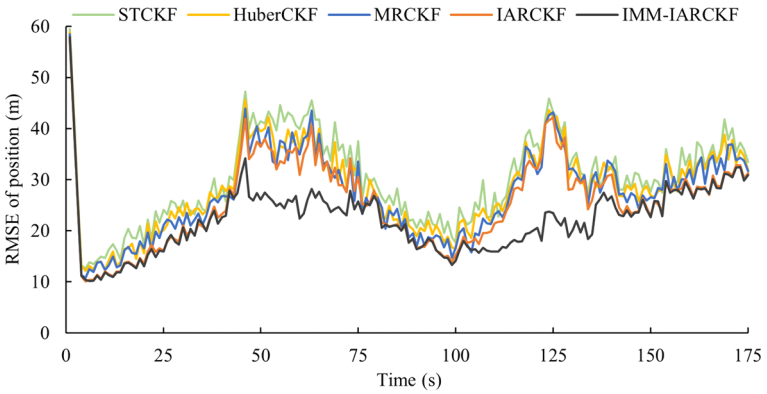

(a) The RMSE of position

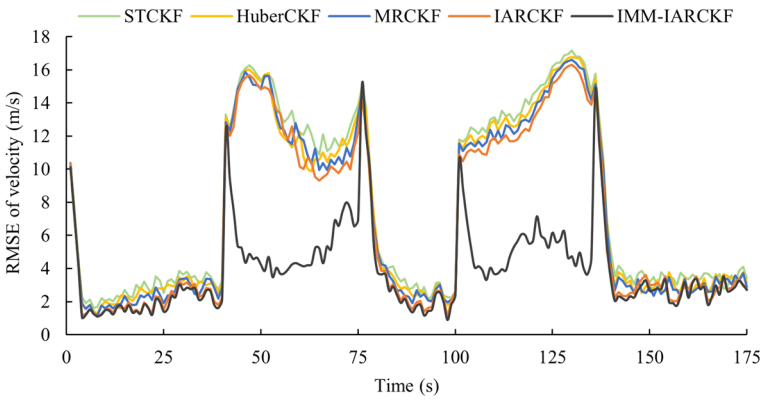

(b) The RMSE of velocity

Fig. 5 The RMSE of different algorithms in position and velocity

3.2.1 The Verification and Analysis of IARCKF Algorithm Performance

The STCKF [29], Huber-CKF [22], and MRCKF [25] algorithms were compared with the proposed IARCKF and IMM-IARCKF algorithms under the above simulation scenario, and the tracking performance of each algorithm was analyzed. The RMSE of five algorithms in position and velocity are displayed in Fig. 5a, b, respectively, and the corresponding tracking accuracy data are presented in Table 3 and Fig. 6, not considering the initial abnormal errors in the simulation experiment.

According to the simulation results in Fig. 5a, b, the tracking performance of the five algorithms was analyzed. In the first four noninteractive filtering algorithms, the IARCKF algorithm achieved the highest estimation accuracy, the Huber-CKF algorithm achieved an approximate estimation accuracy to the MRCKF, and the STCKF obtained the lowest estimation accuracy. In the case of substantial motion state changes

of the target, the RMSE of the above four noninteractive filtering algorithms in position and velocity increased and failed to quickly converge, which was attributed to motion model mismatch and measurement outliers caused by the substantial change in the motion state of the target. Compared with the other three noninteractive filtering algorithms, the IARCKF obtained the optimal estimation accuracy and error convergence effect after wide-range maneuvering of the target. This occurs because the IARCKF algorithm proposed in this study, which is characterized by strong adaptive robustness, better suppresses the influences of measurement model and motion model errors on estimation accuracy. However, due to the excessive characteristic velocity and turning angle of the vehicle, the change in the motion state of the vehicle target still exceeds the limit of the robust estimation ability of the IARCKF algorithm. The IMM-IARCKF algorithm better solves the problem of motion estimation model mismatching while retaining the adaptive robust characteristic of the IARCKF algorithm. Hence, the IMM-IARCKF algorithm shows outstanding error convergence performance in the case of substantial changes in the motion state of the target.

Table 3 and Fig. 6 show that IARCKF outperforms the other filtering algorithms in terms of MAPE (2.28%, 2.83%) and RMSE (25.24 m, 6.37 m/s) of the position and velocity in the first four noninteractive filtering algorithms. The STCKF exhibited the worst performance, with MAPEs of the position and velocity of 3.12% and 4.21%, respectively, and the RMSEs of the position and velocity were 30.16 m and 8.26 m/s, respectively. The IARCKF algorithm has the highest tracking accuracy among the first four noninteractive filtering algorithms. Compared with the STCKF algorithm, the MAPEs of the IARCKF for the position and velocity increased by 26.92% and 32.78%, respectively, and the RMSEs for the position and velocity increased by 22.88% and 16.31%, respectively. Compared with the Huber-CKF algorithm, the MAPEs of the IARCKF for position and velocity were improved by 21.05% and 21.82%, respectively, and the RMSEs for position and velocity were improved by 12.09% and 14.95%, respectively. Finally, compared with the MRCKF algorithm, the MAPEs of the IARCKF for position and velocity were 13.64% and 17.01% higher, respectively, and the RMSEs for position and velocity were 7.18% and 10.53% higher, respectively. Among all the algorithms involved in the comparison, IMM-IARCKF achieved the best target tracking performance, achieving minimum values of both MAPE and values for position and velocity tracking. Since the interactive multiple model method taking the IARCKF as the model condition for filtering is adopted, the estimation accuracy of the IMM-IARCKF algorithm is better than that of the noninteractive filtering algorithms. Therefore, the IMM-IARCKF can better solve the problem of motion estimation model mismatch when the limit of the adaptive robust estimation ability of the IARCKF algorithm is exceeded.

3.2.2 Verification and Analysis of FLIMM-IARCKF Algorithm Performance

To further verify the advantages of the FLIMM-IARCKF algorithm in terms of the error convergence speed and filtering estimation accuracy in the case of sudden changes in the motion state of the target, the target was tracked using the IMM-CKF [20], IMM-IARCKF, and FLIMM-IARCKF algorithms under the same simulation scenario. The

Table 3 Tracking accuracy of different algorithms

Algorithm name	Means of MAPE		Means of RMSE		Peak values of RMSE	
	Position (%)	Velocity (%)	Position (m)	Velocity (m/s)	Position (m)	Velocity (m/s)
STCKF [29]	3.12	4.21	30.16	8.26	47.22	17.69
Huber-CKF [22]	2.85	3.62	28.71	7.49	45.62	16.87
MRCKF [25]	2.64	3.41	27.18	7.12	42.92	16.52
IARCKF	2.28	2.83	25.24	6.37	41.33	16.11
IMM-IARCKF	1.92	2.06	21.56	3.94	34.20	15.06

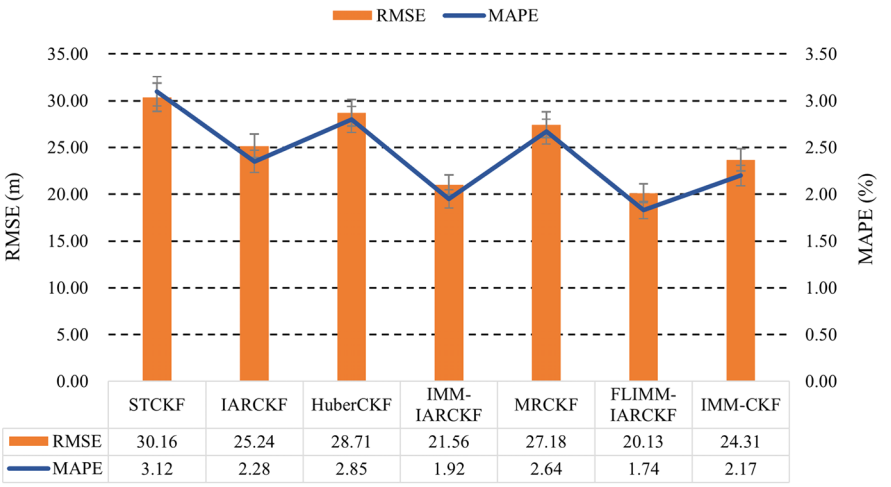

	STCKF	IARCKF	HuberCKF	IMM-IARCKF	MRCKF	FLIMM-IARCKF	IMM-CKF
RMSE	30.16	25.24	28.71	21.56	27.18	20.13	24.31
MAPE	3.12	2.28	2.85	1.92	2.64	1.74	2.17

(a) Tracking accuracy of position

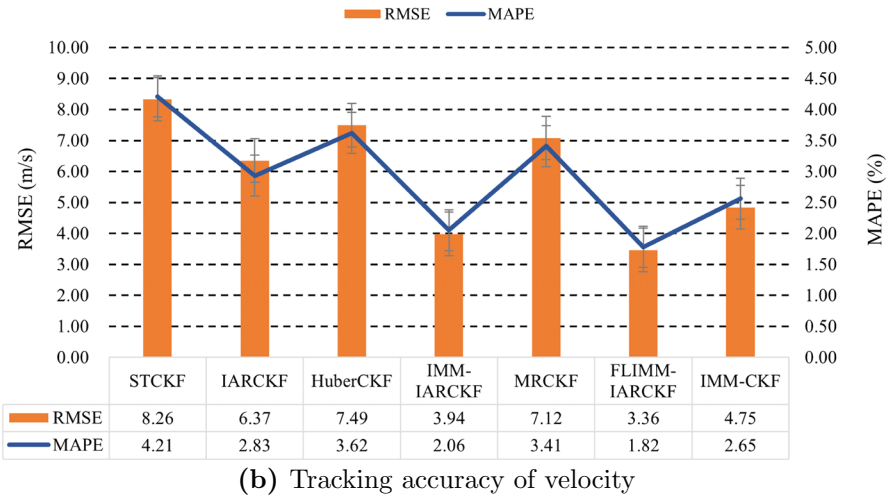

	STCKF	IARCKF	HuberCKF	IMM-IARCKF	MRCKF	FLIMM-IARCKF	IMM-CKF
RMSE	8.26	6.37	7.49	3.94	7.12	3.36	4.75
MAPE	4.21	2.83	3.62	2.06	3.41	1.82	2.65

(b) Tracking accuracy of velocity

Fig. 6 Results of MAPE and RMSE from different algorithms

RMSE of the three algorithms in position and velocity is displayed in Fig. 7a, b, respectively, without considering the initial abnormal errors in the simulation experiment.

Figure 7a, b shows that all three filtering algorithms can avoid the sustained increase in the estimation error through the model interaction after the substantial change in the motion state of the target. However, significant differences were still observed in terms of filtering estimation accuracy and error convergence speed. In the case of a substantial change in the motion state of the target, the tracking performance and estimation error convergence effect of the IMM-IARCKF algorithm were better than those of the IMM-CFK algorithm. This occurs because the model-conditioned filtering

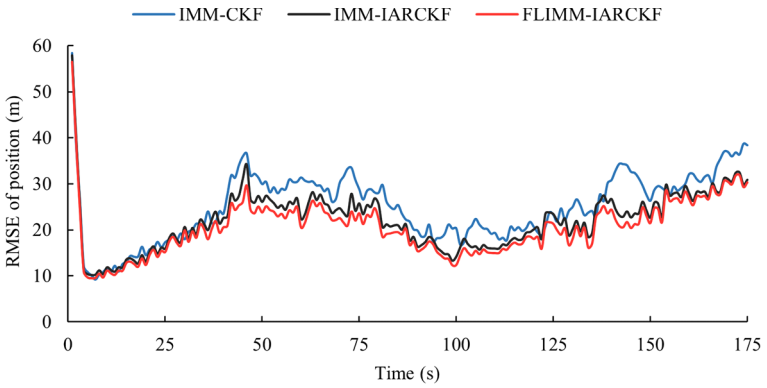

(a) The RMSE of position

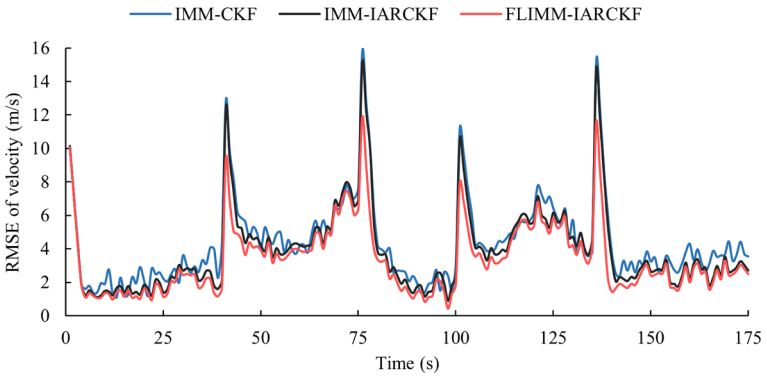

(b) The RMSE of velocity

Fig. 7 The RMSE of different algorithms in position and velocity

of IMM-IARCFK shows superior adaptive robustness characteristics, which can better suppress the influence of the system model error on estimation accuracy. When the vehicle target experiences a sudden change in its motion state, FLIMM-IARCKF can adaptively regulate the process noise covariance coefficient according to the matching degree of the current motion model while improving the probability update response efficiency of the model. Therefore, FLIMM-IARCKF exhibited a smaller estimation error and a faster error convergence speed than IMM-IARCKF, demonstrating that the combined fuzzy reasoning method is efficient.

Table 4 and Fig. 6 reveal that FLIMM-IARCKF outperforms all the competitive filtering algorithms in terms of MAPE (1.74%, 1.82%) and RMSE (20.13 m, 3.36 m/s) of the position and velocity. The error changes and the estimation accuracy of FLIMM-IARCKF are further optimized compared to those of IMM-IARCKF. Compared to the traditional IMM-CKF algorithm, the RMSEs of FLIMM-IARCKF for position and velocity were 17.19% and 29.26% higher than those of IMM-CKF, and the MAPEs of FLIMM-IARCKF for position and velocity were 19.82% and 31.32% higher than

Table 4 Tracking accuracy of different algorithms

Algorithm name	Means of MAPE		Means of RMSE		Peak values of RMSE	
	Position (%)	Velocity (%)	Position (m)	Velocity (m/s)	Position (m)	Velocity (m/s)
IMM-CKF [20]	2.17	2.65	24.31	4.75	38.31	15.81
IMM-IARCKF	1.92	2.06	21.56	3.94	34.20	15.06
FLIMM-IARCKF	1.74	1.82	20.13	3.36	31.68	11.87

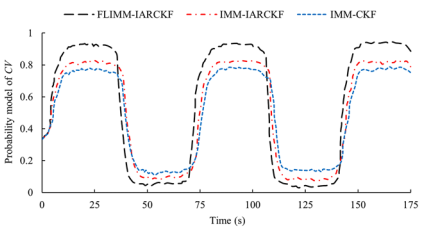

(a) The model probability of CV

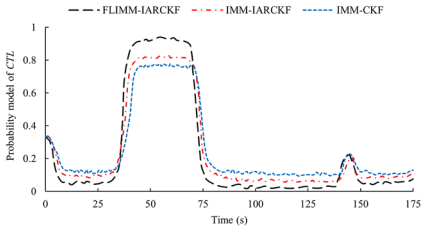

(b) The model probability of CTL

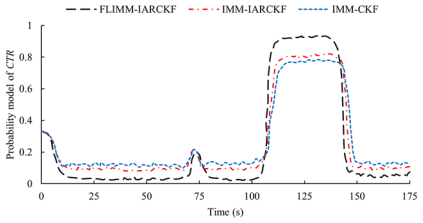

(c) The model probability of CTR

Fig. 8 Model probability of each algorithm under different models

those of IMM-CKF, respectively. The proposed IMM-IARCKF algorithm was compared with the further improved FLIMM-IARCKF algorithm, which revealed that the RMSEs of the FLIMM-IARCKF for position and velocity were 6.63% and 14.72% higher than those of the IMM-IARCKF, and the MAPEs of the FLIMM-IARCKF for position and velocity were 9.38% and 11.65% higher than those of the IMM-IARCKF, respectively.

The model result probabilities of the three algorithms are displayed in Fig. 8. In the case of sudden changes in the motion state of the target, the change rate of the model probability of the FLIMM-IARCKF algorithm was the fastest with the maximum variation range, thus reducing the transition time of model transformation and the competition conflict of model probability. Therefore, the FLIMM-IARCKF algorithm can effectively suppress the influences of the target's motion state changes on the tracking effect and estimation accuracy, improve the response efficiency to model probability updating, and accelerate the rate of error convergence.

4 Real Vehicle Experiment and Verification

To verify the performance advantages and application effect of the FLIMM-IARCKF algorithm in vehicle target tracking under a real scenario, a real vehicle experiment was conducted. Therein, the experimental objects remain the IMM-CKF, IMM-IARCKF, and FLIMM-IARCKF. Conclusions were drawn by comparing the tracking performance and execution efficiency of the algorithms according to the experimental results.

4.1 Establishment of the Experimental Platform

The real vehicle experimental platform consists of a hardware system and a software platform. The integration of the hardware system is established by the millimeter wave radar (Model ARS408-21, 77Ghz, Continental AG, Hannover, Germany), industrial personal computer (IPC, Model NISE3800E, Core i5, Xinhan Inc., Beijing, China), display (Model U2417, HP Inc., CA, USA), CANoe analyzer (Model VN1640A, Vector Inc., Stuttgart, Germany), and laptop (Model OMEN8, Core i7, HP Inc., CA, USA). The IPC communicates with the millimeter wave radar via CAN signals, and the software environment and filtering algorithm of the IPC are deployed through the display. The IPC performs real-time filtering of the target tracking data acquired by the millimeter wave radar and transmits the filtering result, in the form of CAN signals, to CANoe in a real-time fashion. CANoe can acquire all CAN bus data in the experimental process and resolve and save data signals in a timely manner. The CANoe software deployed on the laptop can more intuitively and accurately analyze experimental data. Furthermore, both the experimental vehicle and target vehicle are equipped with a combined inertial navigation system (GNSS/INS, Model SDI-604, ZEDA Inc., Beijing, China) to acquire the position and velocity of the target vehicles. GNSS/INS has centimeter-level measurement accuracy, which can provide a relatively reliable reference value for verifying the estimation accuracy of each filtering algorithm.

The software platform was deployed in the IPC, and the filtering algorithm was established and deployed in the Ubuntu 18.04 operating system via ROS. The ROS Kinetic Kame was installed and configured with related libraries and dependencies, and RoboWare Studio was used as the coding and debugging tool. Moreover, the filtering effect is compared and visualized through the 3D visualization platform (Rviz) of ROS. The construction of a real vehicle experimental platform and the integration of hardware and software are displayed in Fig. 9.

In this experiment, a semitrailer tractor control by-wire carrying the above experimental platform was selected as the experimental vehicle used to track the vehicle target. A millimeter wave radar was installed at the central position of the front bumper of the experimental vehicle, with an installation height of 720 mm from the ground. To prevent the millimeter wave radar from joggling due to the poor rigidity of the fixation position during the experimental period, the millimeter wave radar was fixed on the rigid frame inside the external encirclement of the vehicle. The experimental vehicle deployed with the experimental platform is displayed in Fig. 10a, b.

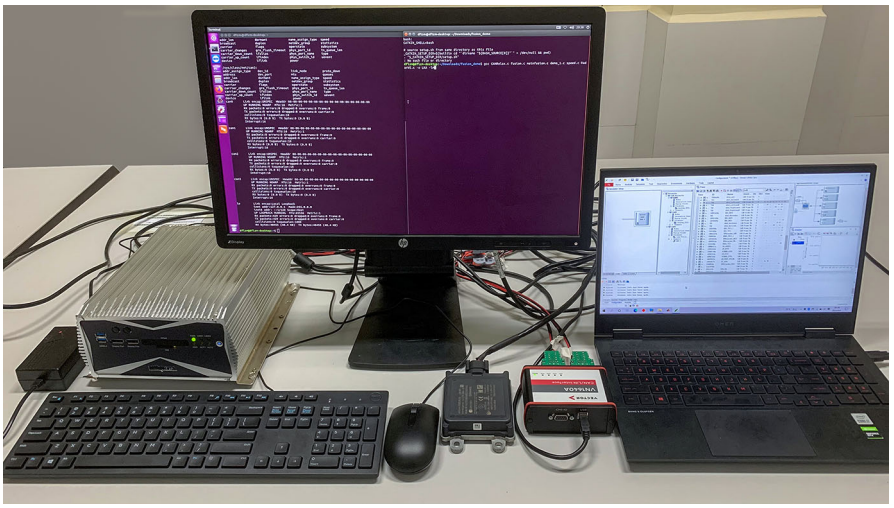

Fig. 9 Construction of a real vehicle experimental platform and integration of hardware and software

(a) Deployment of the experimental platform

(b) Experimental vehicle

Fig. 10 Deployment of the experimental platforms and sensors

4.2 Experimental Methods and Results Analysis

In the experimental process of the experimental vehicle, the average velocity of the target vehicle was approximately 60 km/h, and the experimental vehicle tracked the target vehicle running in front at an approximate running speed. The traveling track of the vehicle target under the inertial coordinate system with the initial running point as the origin is shown in Fig. 11.

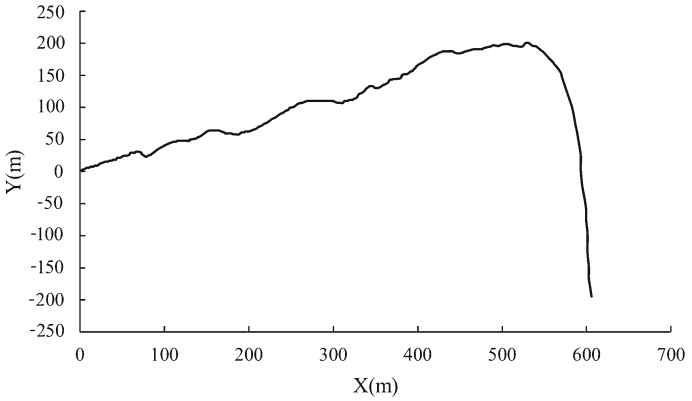

Fig. 11 The traveling track of the vehicle target

To ensure consistency between the experimental environment and conditions, the three filtering algorithms are simultaneously executed under the abovementioned experimental scenario and path to perform the tracking experiment on the vehicle target. The topic communication mechanism of ROS realized the synchronous operation of three filtering algorithm procedures. Moreover, the millimeter wave radar data were preprocessed by screening out the target information and setting the optimal detection range to filter invalid targets in the opposite lane and those beyond the road. The real vehicle experimental results showed the RMSE of the absolute position and velocity of the vehicle in the inertial coordinate system (Fig. 12a, b) as well as the corresponding tracking accuracy data (Table 5).

Analysis of Fig. 12a, b shows that in the real vehicle experiment, the motion state of the target vehicle changed dramatically as it entered the curve, leading to increasing system measurement outliers. Nevertheless, the IARCKF still showed a strong ability to suppress measurement model errors when the vehicle target entered the curve. Furthermore, the FLIMM-IARCKF algorithm displayed a faster error convergence rate and higher estimation accuracy than the IMM-IARCKF. The real vehicle experimental effect further verified the performance characteristics and advantages of FLIMM-IARCKF in vehicle target tracking.

The evaluation indicators in Table 5 further reflect the higher estimation accuracy of the FLIMM-IARCKF algorithm. The results of the real vehicle experiment showed that the RMSE values of FLIMM-IARCKF in absolute position and velocity were 45.16% and 39.08% higher than those of IMM-CKF, and the MAPE values of FLIMM-IARCKF in absolute position and velocity were 36.13% and 32.24% higher than those of IMM-CKF, respectively. Furthermore, the RMSE values of FLIMM-IARCKF in absolute position and velocity were 17.07% and 14.52% higher than those of IMM-IARCKF, and the MAPE improved by 13.79% and 20.63%, respectively.

The radar tracked the maneuvering target at a fixed position in the simulation experiment, and errors might accumulate with the continuous motion of the target, so that the RMSE in the simulation experiment was generally higher than that in the real vehicle experiment. The simulation experiment sought to verify the effectiveness and

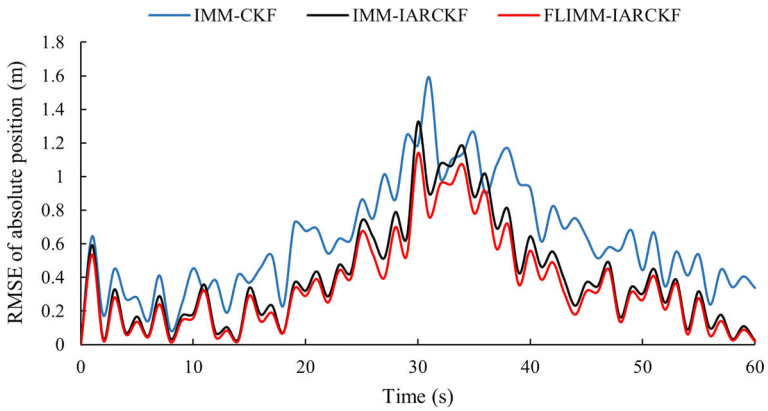

(a) The RMSE of absolute position

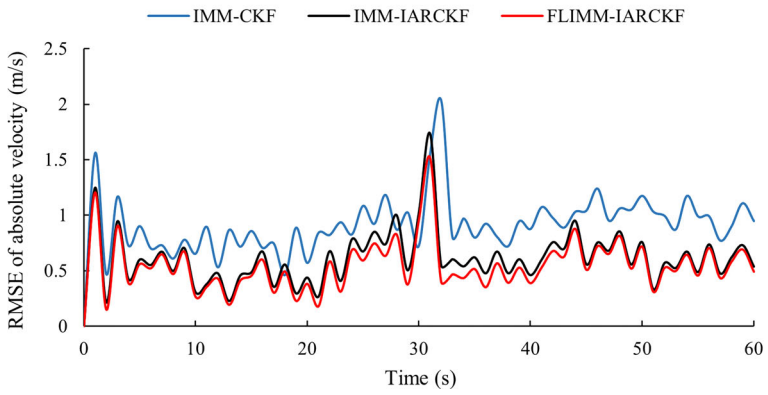

(b) The RMSE of absolute velocity

Fig. 12 The RMSE of absolute position and velocity of the vehicle

accuracy advantages of the proposed algorithm, while its tracking performance under an actual scenario was additionally verified through a real vehicle experiment.

4.3 Algorithm Efficiency Analysis

The complexity of the IMM-CKF, IMM-IARCKF, and FLIMM-IARCKF algorithms was analyzed by floating point operations. The calculation method of complexity can be found in reference [7], which defines the flops of various matrix operations. To analyze the complexity of each algorithm more intuitively, the complexity curves of the three algorithms were drawn according to the complexity calculation results when the dimensions of the state and measurement vectors increased. The complexity curves are shown in Fig. 13a, b, where n and m represent the dimensions of the state and measurement vectors, respectively.

Table 5 Tracking accuracy of each algorithms

Algorithm name	Means of MAPE		Means of RMSE		Peak values of RMSE	
	Absolute position (%)	Absolute velocity (%)	Absolute position (m)	Absolute velocity (m/s)	Absolute position (m)	Absolute velocity (m/s)
IMM-CKF [20]	2.74	3.35	0.62	0.87	1.61	2.06
IMM-IARCKF	2.03	2.86	0.41	0.62	1.35	1.76
FLIMM-IARCKF	1.75	2.27	0.34	0.53	1.14	1.52

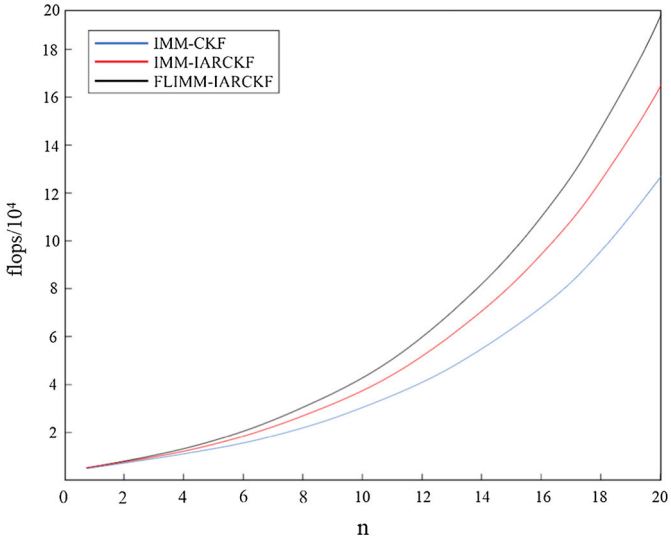

(a) Complexity curve(m=8)

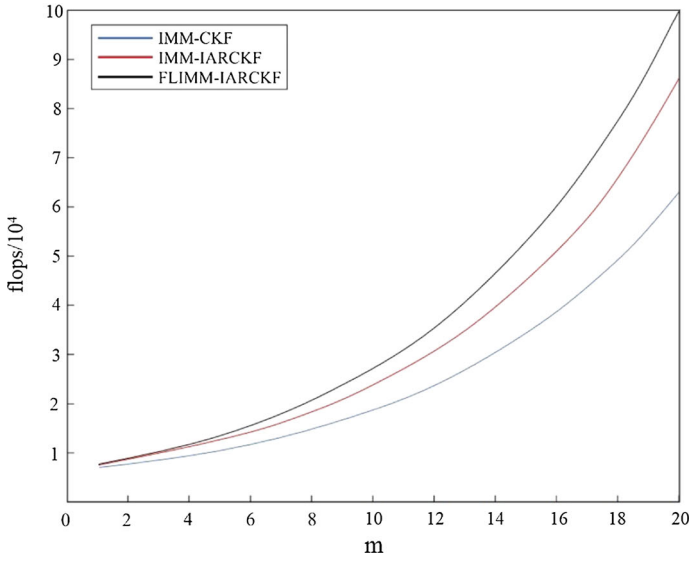

(b) Complexity curve(n=8)

Fig. 13 comparison of complexity among different algorithms

It can be seen by analyzing Fig. 13a, b that the complexity of the FLIMM-IARCKF algorithm is slightly higher than that of the IMM-CKF and IMM-IARCKF when the dimensions of the state and measurement vectors are low. Since the dimensions of the state and measurement vectors are not high under the actual vehicle tracking conditions, the FLIMM-IARCKF algorithm does not introduce a significant loss of efficiency due to the complexity when compared to the traditional IMM-CKF algorithm.

In addition, the execution efficiency of the IMM-CKF, IMM-IARCKF, and FLIMM-IARCKF was comparatively tested to compare their true operating efficiency in the experimental system. This experiment was divided into five groups, in each of which the time spent by each of the three algorithms to operate 1000 consecutive times after being integrated into the IPC of NEXCOM NISE3800E with the Intel Core i5 processor was recorded. The experimental results are listed in Table 6.

The experimental results in Table 6 show that the average took 56.13 ms for the FLIMMIARCKF algorithm to run once and 41.87 ms and 48.82 ms for the IMM-CKF and IMM-IARCKF to run once, respectively. Although the average time consumption of the FLIMM-IARCKF algorithm for single-time operation was slightly higher than that of the other two filtering algorithms, the output period of the continental millimeter wave radar, model ARS408-21, was between 70 and 80 ms, and the execution efficiency of FLIMM-IARCKF could certainly satisfy the real-timeliness requirement of system filtering. Furthermore, the hardware configuration of the system still could have been further optimized, which would provide a sufficient guarantee of adequate computing power to enable the efficient execution of the algorithm.

5 Conclusion

Vehicle target tracking is crucial to target perception and the multisensor fusion of intelligent driving. Measurement outliers and motion estimation model mismatching significantly impact the tracking accuracy of vehicle targets. To suppress the interference of model errors and measurement outliers while improving the accuracy of vehicle target state estimation, an adaptive vehicle target tracking enhancement algorithm based on fuzzy interacting multiple model robust cubature Kalman filtering (FLIMM-IARCKF) is presented. In this algorithm, the cost function of adaptive robust nonlinear filtering is constructed by combining the improved fading factor with a convex robust function. An improved derivative-free adaptive robust cubature Kalman filter is designed based on this cost function, which suppresses the effects of the errors of the measurement model and motion estimation model. Integrating these elements, the combined fuzzy reasoning method is designed to act on the interacting multiple model algorithm, which further enhances the tracking performance and estimation accuracy of the algorithm by adaptively regulating the process noise covariance matrix while increasing the efficiency of model probability updating. Simulated and real-vehicle experiments verify that the FLIMM-IARCKF algorithm demonstrates significant advantages in terms of estimation accuracy, adaptive robustness, and efficiency of model probability updates. The average MAPE and RMSE are increased by

Table 6 Efficiency of algorithm execution

Group number	IMM-CKF(s)	IMM-IARCKF (s)	FLIMM-IARCKF(s)
1	41.93	48.71	56.12
2	41.82	49.08	56.23
3	42.08	48.82	56.27
4	41.83	48.68	55.96
5	41.73	48.79	56.08
Mean value of time	41.87	48.82	56.13

approximately 30% versus competitive algorithms, which verifies the effectiveness of our algorithm and its accuracy for tracking estimation.

Acknowledgements This work was supported by the Guangxi Innovation-driven Development Special Fund Project, China (Grant Nos. AA18242036; AA18242037), and the Zhaoqing University research fund project, China (No. QN202333).

Availability of data and materials The data that support the findings of this study are available from Liuzhou Dongfeng Automobile Company Ltd., but restrictions apply to the availability of these data, which were used under license for the current study and so are not publicly available. Data are, however, available from the authors upon reasonable request and with permission of Liuzhou Dongfeng Automobile Company Ltd.

Declarations

Conflict of interest The authors declare that they have no conflicts of interest.

References

1. L. Chang, B. Hu, G. Chang, A. Li, Multiple outliers suppression derivative-free filter based on unscented transformation. J. Guid. Control. Dyn. **35**(6), 1902–1906 (2012)
2. M. Chen, C. Gao, Z. Ren, Robust covariance and scatter matrix estimation under Huber's contamination model. Ann. Stat. **46**(5), 1932–1960 (2018)
3. Y. Deng, Z. Mo, H. Lu, Robust h_∞ state estimation for a class of complex networks with dynamic event-triggered scheme against hybrid attacks. Chin. Phys. B. **31**(2), 020503 (2022)
4. Z. Deng, L. Yin, B. Huo, Y. Xia, Adaptive robust unscented Kalman filter via fading factor and maximum correntropy criterion. Sensors **18**(8), 2406 (2018)
5. H. Fu, Y. Cheng, C. Cheng, A novel improved cubature Kalman filter with adaptive generation of cubature points and weights for target tracking. Meas. Sci. Technol. **33**(3), 035002 (2021)
6. M.A. Gandhi, L. Mili, Robust Kalman filter based on a generalized maximum-likelihood-type estimator. IEEE Trans. Signal Process. **58**(5), 2509–2520 (2009)
7. M.S. Grewal, *Kalman Filtering: Theory and Practice Using MATLAB*, 2nd edn. (Wiley, New York, 2008)
8. B. Han, H. Huang, L. Lei, C. Huang, Z. Zhang, An improved IMM algorithm based on stsrckf for maneuvering target tracking. IEEE Access **7**, 57795–57804 (2019)
9. D.-J. Jwo, S.-Y. Lai, Navigation integration using the fuzzy strong tracking unscented Kalman filter. J. Navig. **62**(2), 303–322 (2009)

10. K. Kumar, Robust statistics, by PJ Huber & EM Ronchetti [book review]. J. R. Stat. Soc. A. Stat. Ser. A: Stat. Soc. **174**, 241–242 (2011)
11. X.R. Li, V.P. Jilkov, Survey of maneuvering target tracking. Part I. Dynamic models. IEEE Trans. Aerosp. Elec. Syst. **39**(4), 1333–1364 (2003)
12. Y. Li, L. Hou, Y. Yang, J. Tong, Huber's M-estimation-based cubature Kalman filter for an INS/DVL integrated system. Math. Probl. Eng. 2020 (2020)
13. Y. Li, J. Li, J. Qi, L. Chen, Robust cubature Kalman filter for dynamic state estimation of synchronous machines under unknown measurement noise statistics. IEEE Access **7**, 29139–29148 (2019)
14. E. Masazade, M. Fardad, P.K. Varshney, Sparsity-promoting extended Kalman filtering for target tracking in wireless sensor networks. IEEE Signal Proc. Lett. **19**(12), 845–848 (2012)
15. Q. Meng, H. Leib, X. Li, Cubature ensemble Kalman filter for highly dimensional strongly nonlinear systems. IEEE Access **8**, 144892–144907 (2020)
16. J.C. Santos-Leon, R. Orive, D. Acosta, L. Acosta, The cubature Kalman filter revisited. Automatica **127**, 109541 (2021)
17. R. Schubert, C. Adam, M. Obst, N. Mattern, V. Leonhardt, G. Wanielik, Empirical evaluation of vehicular models for ego motion estimation, pp. 534–539 (2011). https://doi.org/10.1109/IVS.2011.5940526
18. J. Shao, W. Chen, Y. Zhang, F. Yu, J. Wang, Adaptive maximum correntropy based robust CKF with variational Bayesian for covariance estimation. Measurement **202**, 111834 (2022)
19. K. Shen, Z. Jing, P. Dong, A consensus nonlinear filter with measurement uncertainty in distributed sensor networks. IEEE Signal Process. Lett. **24**(11), 1631–1635 (2017)
20. R. Song, X. Chen, Y. Fang, H. Huang, Integrated navigation of GPS/INS based on fusion of recursive maximum likelihood IMM and square-root cubature Kalman filter. ISA Trans. **12**(6), 387–395 (2020)
21. M. Sualeh, G.-W. Kim, Dynamic multi-lidar based multiple object detection and tracking. Sensors **19**(6), 1474 (2019)
22. C.-H. Tseng, S.-F. Lin, D.-J. Jwo, Robust huber-based cubature Kalman filter for GPS navigation processing. J. Navig. **70**(3), 527–546 (2017)
23. W. Wan, J. Feng, B. Song, X. Li, Huber-based robust unscented Kalman filter distributed drive electric vehicle state observation. Energies **14**(3), 750 (2021)
24. X. Wang, N. Cui, J. Guo, Huber-based unscented filtering and its application to vision-based relative navigation. IET Radar Sonar Navig. **4**(1), 134–141 (2010)
25. H. Wu, S.-X. Chen, B.-F. Yang, K. Chen, Robust cubature Kalman filter target tracking algorithm based on genernalized M-estiamtion. Acta. Phys. Sin. **64**(21), 218401 (2015). https://doi.org/10.7498/aps.64.218401
26. M. Xu, X. Bu, H. Yang, Dual-band infrared and geomagnetic fusion attitude estimation algorithm based on IMMEKF. IEEE Trans. Ind. Electron. **68**(11), 11286–11295 (2020)
27. Y. Yao, X. Xu, D. Yang, X. Xu, An IMM-UKF aided SINS/USBL calibration solution for underwater vehicles. IEEE Trans. Veh. Technol. **69**(4), 3740–3747 (2020)
28. P. Yun, P. Wu, S. He, X. Li, Robust Kalman filter with fading factor under state transition model mismatch and outliers interference. Circ. Syst. Signal. Proc. **40**(5), 2443–2463 (2021)
29. P. Yun, P. Wu, S. He, X. Li, A variational bayesian based robust cubature Kalman filter under dynamic model mismatch and outliers interference. Measurement **191**, 110063 (2022)
30. D.H. Zhou, P.M. Frank, Strong tracking filtering of nonlinear time-varying stochastic systems with coloured noise: application to parameter estimation and empirical robustness analysis. Int. J. Control **65**(2), 295–307 (1996)
31. B. Zhu, L. Chang, J. Xu, F. Zha, J. Li, Huber-based adaptive unscented Kalman filter with non-gaussian measurement noise. Circ. Syst. Signal. Proc. **37**(9), 3842–3861 (2018)
32. L. Zou, Z. Wang, H. Dong, Q.-L. Han, *Energy-to-peak state estimation with intermittent measurement outliers: The single-output case* (IEEE Trans, Cybern, 2021)

Authors and Affiliations

Guoxin Han[1,2] · Fuyun Liu[1] · Jucai Deng[3] · Weihua Bai[2] · Xiaolin Deng[4] · Keqin Li[5]

Fuyun Liu
liufuyun310@aliyun.com

Jucai Deng
dengjc@dflzm.com

Weihua Bai
bandwerbai@gmail.com

Xiaolin Deng
dengxiaolin3@163.com

Keqin Li
lik@newpaltz.edu

1 College of Mechanical and Electrical Engineering, Guilin University of Electronic Technology, Guilin, China

2 College of Computer Science and Software, Zhaoqing University, Zhaoqing, China

3 Commercial Vehicle Technology Center, Liuzhou Dongfeng Automobile Company Ltd., Liuzhou, China

4 School of Electronics and Information Engineering, Wuzhou University, Wuzhou, China

5 Department of Computer Science, State University of New York New Paltz, New Paltz, NY, USA